Engineering Analysis with Boundary Elements 72 (2016) 27–41

Contents lists available at ScienceDirect

Engineering Analysis with Boundary Elements

journal homepage: www.elsevier.com/locate/enganabound

Analysis of underwater acoustic scattering problems using stable node-based smoothed finite element method

Yingbin Chai [a,b], Wei Li [a,b,c,*], Tianyun Li [a,b,c], Zhixiong Gong [a,b], Xiangyu You [a,b]

[a] School of Naval Architecture and Ocean Engineering, Huazhong University of Science and Technology, Wuhan 430074, China
[b] Hubei Key Laboratory of Naval Architecture and Ocean Engineering Hydrodynamics (HUST), Huazhong University of Science and Technology, Wuhan 430074, China
[c] Collaborative Innovation Center for Advanced Ship and Deep-Sea Exploration (CISSE), Shanghai 200240, China

ARTICLE INFO

Article history:
Received 15 March 2016
Received in revised form
1 July 2016
Accepted 6 August 2016
Available online 17 August 2016

Keywords:
Underwater acoustic scattering
Numerical methods
Finite element method (FEM)
Node-based smoothed finite element method (NS-FEM)
Dirichlet-to-Neumann (DtN) condition

ABSTRACT

A stable node-based smoothed finite element method (SNS-FEM) is presented that cures the "overly-soft" property of the original node-based smoothed finite element method for the analysis of underwater acoustic scattering problems. In the SNS-FEM model, the node-based smoothed gradient field is enhanced by additional stabilization term related to the gradient variance items. It is demonstrated that SNS-FEM provides an ideal stiffness of the continuous system and improves the performance of the NS-FEM and FEM. In order to handle the acoustic scattering problems in unbounded domain, the well known Dirichlet-to-Neumann (DtN) boundary condition is combined with the present SNS-FEM to give a SNS-FEM-DtN model for exterior acoustic problems. Several numerical examples are investigated and the results show that the SNS-FEM-DtN model can achieve more accurate solutions compared to the NS-FEM and FEM.

1. Introduction

Acoustic scattering from objects is an interesting physical phenomena and it is of great importance in various practical application such as underwater acoustics, exploration engineering, non-destructive testing and particle manipulation. During the past few decades, a great number of researches have been conducted regarding this problem. Initial works are mainly focused on the objects with particular geometry where separation of variables is applicable. For example, the exact solutions have been obtained for rigid or elastic spherical solids and shells [1–4], infinite cylinders [1], and spheroids [5,6]. Subsequently, there is a variety of new methods have been developed to solve the acoustic scattering problems. These methods include the perturbation method [7], the Green's function method [8], the *T*-matrix method [9], the Fourier matching method (FMM) based on conformal mapping [10], the boundary integral equations [11] and the partial wave series expansions (PWSE) method [12–15]. However, each of these methods has their own associated advantages, disadvantages and conditions of applicability.

Currently, with the fast development of the computer simulation techniques, the standard finite element method (FEM) and boundary element method (BEM) have been the two most popular and powerful numerical methods in coping with the time-harmonic acoustic scattering problems. The classical BEM can be classified as a boundary discretization method and the main advantage of this method is that only boundary discretization is required. In addition, the BEM can naturally satisfy the required Sommerfeld radiation condition at infinity, while some special treatments are needed when the FEM is used. However, the resulting system equations of BEM are usually non-symmetric and dense, which is opposed to symmetric and banded in FEM. This may increase the processing time and storage requirements. Besides, the potential non-uniqueness of the BEM solution at characteristic wave number values is also an important issue. In the contrast to BEM, the FEM, which are based on variational formulations, has a rich mathematical background and the convergence of FEM to the exact solution is well-proved. There is no theoretical limitation on the applicability of FEM to high wave numbers as long as the sufficient refined mesh is used. Recently a meshless boundary collocation method, the singular boundary method (SBM), has been proposed for exterior acoustic problems [16–18]. In SBM, the concept of source intensity factor is introduced to regularize the singularities of fundamental solutions. It successfully overcomes some shortcomings of the original BEM and can be a good alternative for exterior acoustic problems. However, the mathematical theoretical analysis of the SBM seems to be not as complete as the FEM and the relevant work is still on

* Corresponding author at: School of Naval Architecture and Ocean Engineering, Huazhong University of Science and Technology, Wuhan 430074, China.
E-mail address: hustliw@hust.edu.cn (W. Li).

http://dx.doi.org/10.1016/j.enganabound.2016.08.005
0955-7997/

its way. In the author's opinion, there is no ideal method has been found yet and the quest for such a method will continue.

In fact, the standard FEM for handling the acoustic scattering still remains two major challenges. The first challenge is how to treat the exterior acoustic problems in unbounded domains effectively. As is known to all, FEM has been well developed for acoustic problems in bounded domains. In general, the application of FEM to unbounded domains involves a domain decomposition by introducing an artificial boundary around the objects. At the artificial boundary, the well-known Sommerfeld radiation condition should be satisfied so that there is no spurious wave reflected from the far field. There are various approaches can be combined with the FEM for the analysis of acoustic scattering in unbounded exterior domains, such as the Dirichlet-to-Neumann (DtN) map developed by Keller and Givoli [19], the recursion in the Atkinson-Wilcox expansion devised by Bayliss et al. [20], and the recent perfectly matched layer approach proposed by Bérenger et al. [21–23]. Among them, the DtN boundary condition devised by Givoli and Keller is an exact non-reflecting boundary condition. It relates the "Dirichlet datum" to the "Neumann datum" with the help of an integral operator M. Although this boundary condition is non-local, it still possesses high computational efficiency and can obtain much more accurate results than those obtained from various approximate local conditions. Therefore, the DtN boundary condition is chosen to cope with the exterior acoustic problems in this paper.

Second, when using the standard FEM for the solution of acoustic problems addressed by Helmholtz equation, one soon is confronted with the well-known dispersion error issue. More importantly, the larger wave number k is, the stronger dispersion error will be. Therefore, the standard FEM can only provide reliable numerical results in the small wave number range, when it comes to large wave number range, the FEM solutions will deteriorate quickly due to the dispersion error issue. Initial FEM researchers used the "rule of thumb" to obtain relatively reliable solutions. In this criterion, a certain fixed number of elements are needed to resolve a wavelength. However, this criterion only works well in the small wave number range. With the increase of the wave number, the numerical dispersion error will increase dramatically even if this criterion is satisfied. In order to deal with this dispersion error effectively, a great number of numerical techniques have been tested with varying degree of success.

Based on the standard Galerkin FEM, the Galerkin/least-squares finite element method (GLS) are proposed to tackle the dispersion error issue [24–26]. In the GLS model, the residuals in least-squares form are added to the standard Galerkin variational equation. The numerical results show that the GLS exhibits superior properties for acoustic problems and provides accurate solutions with relatively low dispersion error. Babuška and his colleagues developed a quasi-stabilized FEM (QSFEM) to solve the Helmholtz equations in two or more space dimensions [27,28]. It is demonstrated that the dispersion error can be controlled by the QSFEM. However, the QSFEM model is very complicated in the general setting. Also based on the standard Galerkin FEM, Franca et al. proposed the residual-free-bubbles (RFB) method for Helmholtz equation [29]. Unfortunately, it is found that the RFB is effective in one dimensions but not in higher dimensions. Furthermore, the high-order finite element method has also been applied for acoustic problems [30] and significant improvements on accuracy are achieved, but higher cost in computation. In addition to the standard finite element method and the extended finite element method mentioned above, the meshfree methods have also been introduced to solve the acoustic problems, such as the element-free Galerkin method (EFGM) [31,32], the multi-resolution reproducing kernel particle method (RKPM) [33], the radial point interpolation method (RPIM) [34] and the meshless Galerkin least-square method (MGLS) [35]. Although the calculation accuracy can be improved to a certain extent with these methods, the dispersion error in general two and three dimensional acoustic problems still cannot be properly eliminated.

As mentioned in reference [36], the approximate discrete model may be the main reason to cause dispersion error. The stiffness of the discretized model obtained from the standard FEM always behaves stiffer than the original model, leading to the so-called numerical dispersion error. So producing a properly "softened" stiffness for the discrete model is much more essential to control the numerical error. Recently, Liu et al. have proposed a series of smoothed finite element methods (S-FEM) which are formulated by incorporating the gradient smoothing techniques of meshfree methods into the existing standard FEM [37–40]. The S-FEMs have been applied to analyze linear elastic solid mechanics and it is found that S-FEMs possess excellent features. Recently, the S-FEMs have been successfully applied to solve acoustic and coupled structural-acoustic problems [41–45]. In the S-FEM family, the node-based smoothed finite element method (NS-FEM) is formulated by performing the gradient smoothing technique over the smoothing domains associated with nodes [46–48]. The numerical results demonstrate that the NS-FEM can provide an upper bound in the strain energy of the exact solution when a reasonably fine mesh is used. However, NS-FEM is temporally instable and cannot be applied to solve the dynamic problems and acoustic problems directly due to its "overly-soft" property. In order to overcome the temporal instability of the NS-FEM, Cui et al. have proposed the stable node-based smoothed finite element method (SNS-FEM) for elasticity problems and acoustic problems [49,50]. In the SNS-FEM, a extra gradient variance item is added to the smoothed gradient field. It is found that SNS-FEM possesses an ideal stiffness of the continuous system and improves the performance of the NS-FEM and FEM. In the present research, the SNS-FEM is used to solve the underwater acoustic scattering problems which are very important in various scientific fields such as linear and nonlinear wave mechanics, underwater technology and ocean acoustics. In this paper, the SNS-FEM is combined with the DtN boundary condition to give a SNS-FEM-DtN model for acoustic scattering problems. Due to the good performance of the SNS-FEM in interior acoustic problems and elasticity problems, it is expected that the SNS-FEM can solve the acoustic scattering problems with very exact solutions.

2. The exterior boundary value problem for the Helmholtz equation

Consider an infinite acoustic problem domain with homogeneous isotropic medium. The acoustic wave satisfies the following reduced wave equation (or the Helmholtz equation).

$$\Delta p + k^2 p = f \tag{1}$$

where p is the acoustic pressure, k is the wave number, Δ is the Laplace operator and f is the acoustic source term.

Assuming that the surface of the obstacle immersed in the unbounded domain can be decomposed into Dirichlet boundary condition Γ_p and Neumann boundary condition Γ_v, where $\Gamma_p \cap \Gamma_v = \varnothing$. The Dirichlet boundary condition and Neumann boundary condition can be described as follows:

$$p = p_D \quad \text{on } \Gamma_p \tag{2}$$

$$\nabla p \cdot n = -j\rho\omega v_n \quad \text{on } \Gamma_v \tag{3}$$

where $j = \sqrt{-1}$, ρ is the density of the medium, ω is the angular

frequency and v_n is the normal velocity on the boundary.

In order to ensure that there is no spurious wave reflected from the far field, the well-known Sommerfeld radiation condition should be satisfied.

$$\lim_{x\to\infty} r^{\frac{(d-1)}{2}}\left(\frac{\partial p}{\partial r} - ikp\right) = 0 \tag{4}$$

where d is the number of space dimensions.

3. The FEM-DtN method

The exterior boundary value problem governed by Eqs. (1)–(4) cannot be solved directly by the standard finite element method because the problem domain is infinite. In order to overcome this difficulty, an artificial boundary, which is often a d-dimensional sphere, is usually introduced into this problem. As shown in Fig. 1, the original infinite domain is decomposed into two parts by the artificial boundary B. The external part is still infinite and it can be solved by the analytical approach. The internal part is finite and all the surface of the obstacle is contained within it. The internal part can be solved by the finite element method.

For the external part with an arbitrary Dirichlet boundary condition on the artificial boundary, the analytical solution can be obtained. In two dimensions, according to Keller and Givoli [19], the analytical solution of this problem can be expressed as:

$$p(r,\theta) = \frac{1}{\pi}{\sum_{n=0}^{\infty}}' \int_0^{2\pi} \frac{H_n^{(1)}(kr)}{H_n^{(1)}(kR)} \cos\ n(\theta-\theta')p(R,\theta')\mathrm{d}\theta' \tag{5}$$

where R is the radius of the circular artificial boundary, $p(R,\theta')$ is the acoustic pressure on the artificial boundary, the prime after the sum indicates that a factor of 1/2 multiples the term with $n=0$, $H_n^{(1)}$ is the Hankel function of the first kind.

For the internal part, the problem domain is bounded and so it could be solved by the standard finite element method. We now proceed to formulate the Galerkin weak form of this problem. As mentioned in the previous section, the strong form of this problem is given by Eqs. (1)–(4). The weighted residual equation can be obtained by multiplying with a test function w and integrating over the entire domain. Using Green's theorem, the Galerkin weak form for this problem can be obtained by:

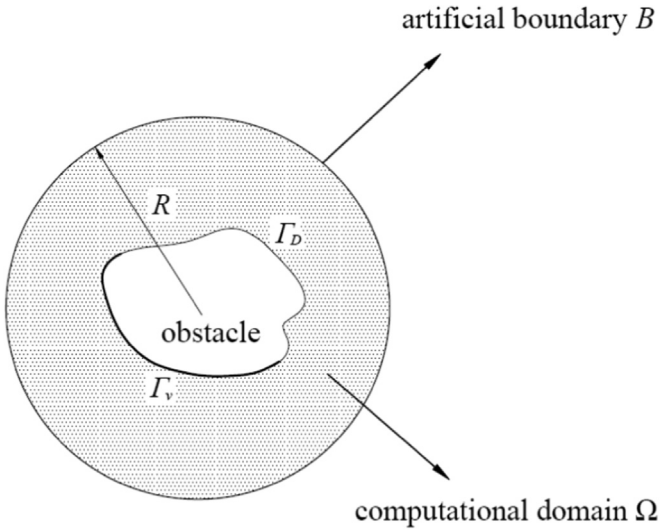

Fig. 1. The infinite domain is usually truncated by an artificial boundary B yielding a finite computational domain Ω.

$$\int_\Omega \left(k^2 wp - \nabla w\cdot\nabla p\right)\mathrm{d}\Omega + \int_B w\frac{\partial p}{\partial n}\mathrm{d}B = \int_\Omega fw\mathrm{d}\Omega + \int_\Gamma v_n w\mathrm{d}\Gamma \tag{6}$$

From Eq. (6), it is seen that the normal derivative of the acoustic pressure $\frac{\partial p}{\partial n}$ on the artificial boundary is not yet known. Therefore, the main problem at this stage is how to calculate the integral $\int_B w\frac{\partial p}{\partial n}\mathrm{d}B$. Here the well-known DtN map is used to handle this problem. In the DtN method, the normal derivative $\frac{\partial p}{\partial n}$ (the Neumann datum) on the artificial boundary can be replaced by the acoustic pressure p (the Dirichlet datum) and the DtN operator M.

$$\frac{\partial p}{\partial n} = -Mp \quad \text{on} \quad B \tag{7}$$

As mentioned in the previous section, the analytical solution for the external part is available. By differentiating Eq. (5) with respect to r and setting $r=R$, we obtain

$$p_v = \left.\frac{\partial p(r,\theta)}{\partial n}\right|_{r=R} = -{\sum_{n=0}^{\infty}}' \int_0^{2\pi} m_n(\theta-\theta')p(R,\theta')\mathrm{d}\theta' \tag{8}$$

where

$$m_n(\theta-\theta') = -\frac{k}{\pi}\frac{H_n^{(1)'}(kR)}{H_n^{(1)}(kR)}\cos\ n(\theta-\theta') \tag{9}$$

in which $m_n(\theta-\theta')$ is the DtN kernels and it can be separated as

$$m_n(\theta-\theta') = -\frac{k}{\pi}\frac{H_n^{(1)'}(kR)}{H_n^{(1)}(kR)}\left(\cos\ n\theta\ \cos\ n\theta' + \sin\ n\theta\ \sin\ n\theta'\right) \tag{10}$$

In this manner, the original problem in infinite domain can be solved successfully. The detailed formulation of this problem by finite element method is not given in this paper, interested readers may refer to reference [36]. According to Keller and Givoli [19], the discretized system equation for this problem can be obtained in the following matrix form:

$$\mathbf{Kp} = \mathbf{F} \tag{11}$$

where $\mathbf{K}$ is the system stiffness matrix, $\mathbf{p}$ is the unknown nodal acoustic pressure in the computational domain, $\mathbf{F}$ is the vector of nodal force.

The system stiffness matrix $\mathbf{K}$ can be written in two parts:

$$\mathbf{K} = \mathbf{K}^a + \mathbf{K}^b \tag{12}$$

where

$$\mathbf{K}^a = \left[\mathbf{K}_{IJ}^a\right] \quad \mathbf{K}^b = \left[\mathbf{K}_{IJ}^b\right] \tag{13}$$

$$\mathbf{K}_{IJ}^a = a(N_I,N_J) = \int_\Omega (\nabla\mathbf{N})^T\nabla\mathbf{N}\mathrm{d}\Omega - k^2\int_\Omega \mathbf{N}^T\mathbf{N}\mathrm{d}\Omega \tag{14}$$

$$\mathbf{K}_{IJ}^b = b(N_I,N_J) \tag{15}$$

where $\mathbf{K}^a$ can be derived from the first term of Eq. (6), $\mathbf{K}^b$ contains the DtN boundary condition and can be derived from the second term of Eq. (6), I and J denote the node number and N_I is the defined shape function for node I.

By substituting Eq. (8) into Eq. (7), the stiffness matrix $\mathbf{K}^b$ which contains the DtN operator M can be obtained as:

$$\begin{aligned}\mathbf{K}_{IJ}^b = b(N_I,N_J) &= \int_B \mathbf{N}_I M\mathbf{N}_J\mathrm{d}B \\ &= -{\sum_{j=0}^{\infty}}'\frac{k}{\pi}\frac{H_n^{(1)'}(kR)}{H_n^{(1)}(kR)}\left(\int_B \mathbf{N}_I(\mathbf{x})\mathbf{F}_j(\mathbf{x})\mathrm{d}B\right)\left(\int_B \mathbf{N}_J(\mathbf{x})\mathbf{F}_j(\mathbf{x}')\mathrm{d}B\right)\end{aligned} \tag{16}$$

where the simple trigonometric functions $F_j(\mathbf{x})$ and $F_j(\mathbf{x}')$ are determined by:

$$\mathbf{F}_j(\mathbf{x}) = \begin{bmatrix} \cos\ n\theta & \sin\ n\theta \end{bmatrix} \tag{17}$$

$$\mathbf{F}_j(\mathbf{x}') = \begin{bmatrix} \cos\ n\theta' \\ \sin\ n\theta' \end{bmatrix} \tag{18}$$

It can be seen from Eq. (12) that the effect of the DtN boundary condition on the standard finite element method is the inclusion of the matrix $\mathbf{K}^b$ in the system stiffness $\mathbf{K}$. Due to the local support property of the FEM shape functions, the value of $\mathbf{N}_I$ equals 1 at node I and equals 0 at every other node. Besides, $\mathbf{N}_I$ will vanish outside a local patch of elements which share node I. Then the matrix $\mathbf{K}^b_{IJ}$ is nonzero only if both nodes I and J lie on the boundary B. The matrix $\mathbf{K}^b_{IJ}$ corresponds to DtN boundary condition. After having calculated $\mathbf{K}^b_{IJ}$, the exterior acoustic problems in unbounded domain can be solved by the standard finite element scheme.

It should be noted that both the radius of the artificial boundary (R) and the number of terms used in the DtN map (N) can affect the accuracy of the numerical solution. The accuracy of solution will improve with the increasing of the two parameters. However, large values of R will always lead to expensive computational cost. On the other hand, if the value of R is too small, large round-off errors will deteriorate the accuracy of the numerical solution. In addition, the full DtN map is represented by infinite series. In practice, the infinite series have to be truncated at some limit. With the increasing of the number of terms used, the truncation error will become smaller. Actually, for fixed R and the average mesh size h, there exist a N which is optimal (N_{opt}). This value N_{opt} occurs when the finite element discretization error equals the truncation error. According to Keller and Givoli [19], the value of R and N_{opt} can be determined by the following formula:

$$N_{\text{opt}} = -(p+1)\frac{\log_{10}(h)}{\log_{10}(R)} \tag{19}$$

where p is the degree of polynomial approximation used in the numerical methods.

In the present work, unless otherwise specified, $N=30$ and $R=1$ is choosed in the practical computation. Numerical examples demonstrate that the chosen values of the two parameters is sufficient to ensure the accuracy of the numerical solution.

4. Formulation of the stable node-based smoothed finite element method (SNS-FEM)

4.1. Brief on the node-based smoothed finite element method (NS-FEM)

In the NS-FEM model, the problem domain Ω is first divided into N_e triangular elements with N_n nodes. Based on these triangular elements, the node-based smoothing domains are created by sequentially connecting the mid-edge-points with centroids of the surrounding triangles. The smoothing domain associated with node k is labeled as Ω_k^s and Γ_k^s is the boundary of Ω_k^s, as shown in Fig. 2. The gradient smoothing technique is utilized here and the integration required in Eq. (14) is now performed over the smoothing domains rather than the original triangular elements.

For acoustic problems, the acoustic particle velocity v in ideal fluid is linked to the gradient of acoustic pressure p by the following equation.

$$\nabla p + j\rho\omega v = 0 \tag{20}$$

In this present formulation, the acoustic particle velocity v is

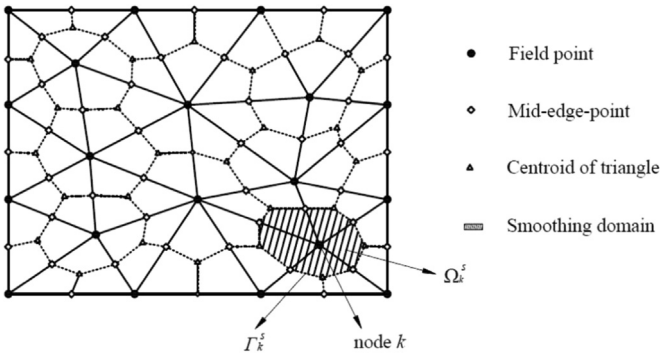

Fig. 2. The node-based smoothing domains in 2D problem are created by sequentially connecting the mid-edge-point to the centroids of surrounding n-sided polygonal elements.

smoothed by the node-based gradient smoothing technique and the smoothed velocity field $\bar{\mathbf{v}}(\mathbf{x})$ in the smoothing domain Ω_k^s can be obtained by:

$$\bar{\mathbf{v}}(\mathbf{x}) = \frac{1}{A_k^s}\int_{\Omega_k^s} \mathbf{v}(\mathbf{x})\mathrm{d}\Omega \tag{21}$$

Using the relationship between the acoustic particle velocity v and acoustic pressure p, and introducing the Green's divergence theorem, the smoothed velocity field presented in Eq. (21) can be obtained in terms of the acoustic pressure p.

$$\begin{aligned}\bar{\mathbf{v}}(\mathbf{x}) &= \frac{1}{A_k^s}\int_{\Omega_k^s} \mathbf{v}(\mathbf{x})\mathrm{d}\Omega = -\frac{1}{j\rho\omega A_k^s}\int_{\Omega_k^s} \nabla p \mathrm{d}\Omega \\ &= -\frac{1}{j\rho\omega A_k^s}\int_{\Gamma_k^s} p\cdot n \mathrm{d}\Gamma\end{aligned} \tag{22}$$

in which A_k^s is the area of smoothing domain Ω_k^s.

In this work, the simple linear shape function is used and the smoothed velocity $\bar{\mathbf{v}}(\mathbf{x})$ can be rewritten in the following matrix form:

$$\bar{\mathbf{v}}(\mathbf{x}) = -\frac{1}{j\rho\omega}\sum_{i\in M_k} \bar{\mathbf{B}}_i(\mathbf{x}) p_i \tag{23}$$

in which M_k is the total number of nodes in the influence domain of node k.

Implementing the Gauss integration scheme along the boundary Γ_k^s, the smoothed gradient matrix presented in Eq. (23) can be calculated as:

$$\bar{\mathbf{B}}_i(\mathbf{x}) = \frac{1}{A_k^s}\sum_{q=1}^{N_s}\left(\sum_{r=1}^{N_g} w_r \mathbf{N}_I(x)\begin{bmatrix} n_x \\ n_y \end{bmatrix}\right) \tag{24}$$

where N_s is the number of segments of the boundary Γ_k^s, N_g is the number of the Gauss points distributed in each segment and w_r is the corresponding weight coefficients for Gauss point, n_x and n_y are the components of the outward normal vector on the boundary Γ_k^s.

Then the smoothed element stiffness matrix for smoothing domain Ω_k^s can be obtained as:

$$\bar{\mathbf{K}}^{(k)} = \int_{\Omega_k^s} \bar{\mathbf{B}}^T\bar{\mathbf{B}}\mathrm{d}\Omega = \bar{\mathbf{B}}^T\bar{\mathbf{B}}A_k^s \tag{25}$$

Finally, the global smoothed element stiffness matrix can be assembled using

$$\bar{\mathbf{K}}^{\text{NS-FEM}} = \sum_{k=1}^{N_n}\bar{\mathbf{K}}^{(k)} \tag{26}$$

5. The stabilized gradient smoothing technique for NS-FEM

In the original NS-FEM model, the smoothed gradient fields are obtained by implementing the numerical integration over the node-based smoothing domains. The bandwidth of stiffness matrix for the NS-FEM model is larger than the FEM model because more nodes are needed in each node-based smoothing domain. The numerical results demonstrated that the NS-FEM can provide an upper bound in the strain energy of exact solution for the solid mechanics problems. However, the NS-FEM also suffers from the "overly-soft" property which makes the NS-FEM temporally instable. In fact, the NS-FEM cannot be used directly to solve dynamic problems and nonlinear problems due to the temporal instability property. More importantly, the authors find that the NS-FEM always leads to non-converging numerical results for acoustic problems, when it comes to exterior acoustic problems, this phenomenon will be even more severe. In order to overcome this deficiency, some special stabilization techniques are needed for the original NS-FEM. An effective stabilization scheme which can improve the performance of NS-FEM will be presented in this section.

Because the linear shape function is used here, the gradient of acoustic is constant in each sub-smoothing domain Ω_k^s and different from element to element. Such a piecewise constant gradient field obviously cannot represents very well the exact gradient field, and should be somehow modified or corrected. To make a proper correction, the changes of acoustic pressure gradient should be considered. In practical computation, this idea can be implemented by the following steps.

Assuming each node-based smoothing domain can be approximated as a circle domain Ω_k^{sc} with the same area A_k^s. It is then divided into four sub-domains, the selected integration points g_n $(n=1, 2, 3, 4)$ lie in x-axis and y-axis, and keep the same distance r_c to node k, as shown in Fig. 3. The radius of the approximate domain can be calculated by

$$r_c = \sqrt{A_k^s/\pi} \tag{27}$$

Assuming that the acoustic gradient in Ω_k^{sc} is continuous and differentiable at the first order, its Taylor expansion can be written as

$$\nabla p = (\nabla p)_k + \frac{\partial(\nabla p)}{\partial x}(x - x_k) + \frac{\partial(\nabla p)}{\partial y}(y - y_k) \tag{28}$$

Then the acoustic pressure gradient at the four selected integration points can be obtained by

$$(\nabla p)_{k_1}^{sc} = (\nabla p)_k^s - \frac{(\nabla p)}{\partial x}\cdot r_c \quad (\nabla p)_{k_3}^{sc} = (\nabla p)_k^s + \frac{(\nabla p)}{\partial x}\cdot r_c \tag{29}$$

$$(\nabla p)_{k_2}^{sc} = (\nabla p)_k^s - \frac{(\nabla p)}{\partial y}\cdot r_c \quad (\nabla p)_{k_4}^{sc} = (\nabla p)_k^s + \frac{(\nabla p)}{\partial y}\cdot r_c \tag{30}$$

Substituting Eqs. (29) and (30) into Eq. (14), the modified smoothed stiffness matrix over the smoothing domain can be obtained by

$$\begin{aligned}\widehat{\mathbf{K}}_k^s &= \frac{1}{4}A_k^s\sum_{g=1}^{4}\left(\bar{\mathbf{B}}_{k,g}^s\right)^T\left(\bar{\mathbf{B}}_{k,g}^s\right)\\ &= \bar{\mathbf{K}}_k^s + \frac{1}{2}A_k^s\left(\bar{\mathbf{B}}_k^s\right)_x^T\left(\bar{\mathbf{B}}_k^s\right)_x + \frac{1}{2}A_k^s\left(\bar{\mathbf{B}}_k^s\right)_y^T\left(\bar{\mathbf{B}}_k^s\right)_y\end{aligned} \tag{31}$$

in which $\bar{\mathbf{K}}_k^s$ is the same as in Eq. (25) and the additional gradient matrix $\left(\bar{\mathbf{B}}_k^s\right)_m$ $(m=x, y)$are obtained by

$$\left(\bar{\mathbf{B}}_k^s\right)_m = \frac{\partial\left(\bar{\mathbf{B}}_k^s\right)}{\partial m}\cdot r_c \quad (m = x,\ y) \tag{32}$$

From Eq. (31), it is found that the NS-FEM model has been strengthen by the addition of terms that contain the changes of acoustic pressure gradient in the smoothing domain. The "overly-soft" deficiency of the original NS-FEM may be cured by the above procedure and it is reasonable to expect that the performance of NS-FEM could be improved for acoustic problems.

6. Numerical error estimates in acoustic problems

As is well known, both the wave number k and the average mesh size h of the numerical model can influence the quality of the numerical solution for acoustic problems using FEM. In practical application, the so-called "the rule of thumb" is usually used to obtain relatively reliable solutions. According to this criterion, a wave-length should always be resolved by a certain fixed number of elements. However, this criterion can only work well in the small wave numbers range. With the increase of the wave numbers, the numerical dispersion error will increase quickly even if this criterion is satisfied.

As the published literature mentioned [51], the numerical error indicator in the H^1-semi-norm can be expressed as:

$$e_n^2 = \left|p^e - p^h\right|^2 = \int_\Omega \left(\tilde{v}^e - \tilde{v}^h\right)^{\mathrm{T}}\left(v^e - v^h\right)\mathrm{d}\Omega \tag{33}$$

where $\tilde{v}$ is the complex conjugate of the velocity, the superscript e denotes the exact solutions and h denotes the numerical solutions obtained from numerical methods including the present SNS-FEM and standard FEM.

It is proved that the relative error of the hp-version FEM solution for acoustic problems in H^1-semi-norm is bounded by [51]:

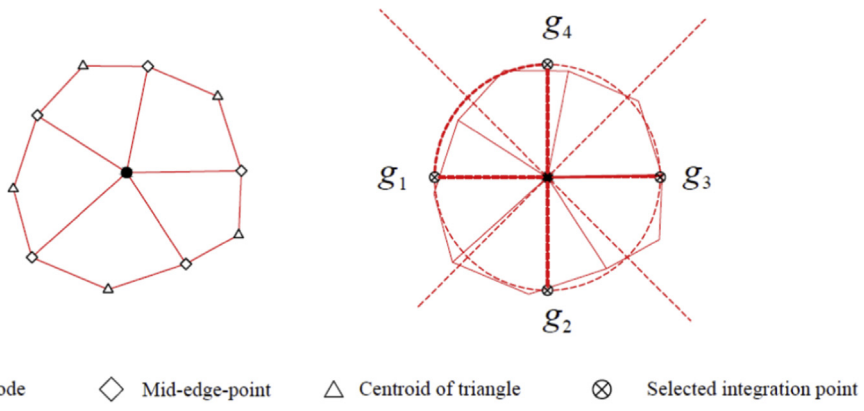

Fig. 3. The schematic of approximate integration domain and selected integration points for SNS-FEM in two-dimensional space.

$$\eta = \frac{|p^e - p^h|}{|p^e|} = \sqrt{\frac{\int_\Omega (\tilde{v}^e - \tilde{v}^h)^{\mathrm{T}} (v^e - v^h) \mathrm{d}\Omega}{\int_\Omega (\tilde{v}^e \cdot v^e)^2 \mathrm{d}\Omega}} \leq C_1 \left(\frac{kh}{p}\right)^p + C_2 k \left(\frac{kh}{p}\right)^{2p} \tag{34}$$

where p is the degree of polynomial approximation used in the numerical methods.

In this paper, the linear shape functions ($p = 1$) are employed, the relative error η can be rewritten as

$$\eta \leq C_1 kh + C_2 k^3 h^2 \tag{35}$$

From Eq. (34), it can be seen that the numerical error can be split into two parts, namely the numerical interpolation error and the numerical pollution error. The first term in Eq. (35) is the interpolation error and it is obvious that this numerical error can be controlled by keeping kh constant. The second term in Eq. (35) is the numerical pollution error caused not only by phase shift but also the error on the amplitude of the wave and this numerical error can be controlled by keeping k^3h^2 constant.

For linear interpolation ($p = 1$) discussed in this paper, the pollution error is neglectable if $kh < 1$, so the major component of the relative error is the interpolation error for small wave numbers. However, when it comes to large wave numbers, the pollution error will dominate the relative error, because it will increase quickly with the increase of wave number k. In this present paper, the two-dimensional acoustic scattering problems are analyzed and the relative error of the numerical solution obtained from the standard FEM and SNS-FEM will be discussed in details.

7. Numerical results

In this section, a number of typical numerical examples are conducted to illustrate the performance and ability of the proposed SNS-FEM for acoustic scattering problems. For the purpose of comparison, the corresponding numerical results obtained from the Galerkin/least-squares finite element method (GLS) are also available in this section. Numerical results showed that the present SNS-FEM can successfully cure the "overly-soft" property of the original NS-FEM and achieve convergent results. More importantly, the SNS-FEM can provide much more accurate results than the standard FEM and GLS, and the numerical error is significantly decreased.

7.1. The circular scatterer

The first numerical example considered here is the acoustic scattering by a rigid infinite circular cylinder in water. As shown in Fig. 4, the direction of the incident plane acoustic wave is along

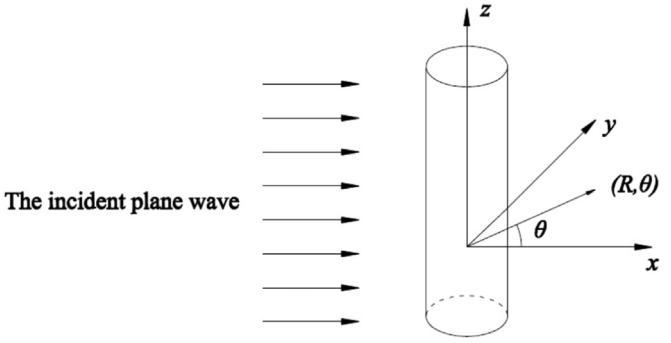

Fig. 4. The acoustic scattering from a single rigid cylinder with infinite length located in the unbounded domain.

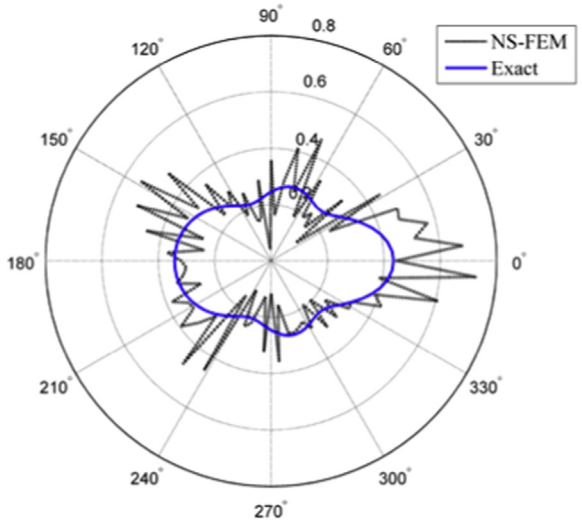

Fig. 5. The scattering patterns of total pressure at wave number $k = 10$ of the circular cylinder using the original NS-FEM model.

x-axis. The density of the fluid around the cylinder is 1000 kg/m^3 and the velocity of the acoustic wave 1500 m/s. Such a problem can be considered as a two dimensional acoustic scattering problems even if it is a three dimensional problem because one of its dimensions is quite larger than the two other ones. The circular obstacle with radius a=0.2 is located at (0, 0). The artificial boundary B with the center at (0, 0) is a circle with radius R=1. The analytical solution for this acoustic scattering problem is available and the scattered acoustic pressure field can be expressed as

$$p = \sum_{n=0}^{\infty} \left[-(-j)^n \varepsilon_n \frac{\frac{\mathrm{d}}{\mathrm{d}(ka)} J_n(ka)}{\frac{\mathrm{d}}{\mathrm{d}(ka)} H_n^{(2)}(ka)} \right] H_n^{(2)}(kr)\cos(n\theta) \tag{36}$$

where k is the wave number, $J_n(x)$ denotes the Bessel function of the first kind, $H_n(x)$ denotes the Hankel function of the second kind. θ is the scattering angle. In Eq. (36), when $n = 0$, $\varepsilon_n = 1$, otherwise $\varepsilon_n = 2$.

7.1.1. Accuracy of the scattered acoustic field

Fig. 5 shows the scattering patterns of total pressure at wave number $k = 10$ of the circular cylinder using the original NS-FEM model. From the figure, it is clearly seen that the NS-FEM results for the acoustic scattering problems is non-converging. The possible reason for this phenomenon may be that the original NS-FEM model suffers from the "overly-soft" property and it cannot be used directly to solve acoustic scattering problems. In order to overcome this issue, the original NS-FEM model should be properly modified. The SNS-FEM model proposed in this paper is expected to meet this need.

At first, three different wave number values ($k = 5$, $k = 10$ and $k = 15$) have been employed to study this typical acoustic scattering field using the proposed SNS-FEM with average mesh size of 0.04 m. For comparison, the FEM and GLS results are also computed using the same mesh. The scattering patterns of total pressure at a distance of r=1 m at different wave numbers for the circular cylinder are shown in Fig. 6. In order to test the performance of the SNS-FEM method, the FEM and GLS results, together with the exact solutions, are also plotted in the figures. From these figures, we can clearly observe the following:

1. The "overly-soft" property of the original NS-FEM model has been cured and the proposed SNS-FEM can provide convergent

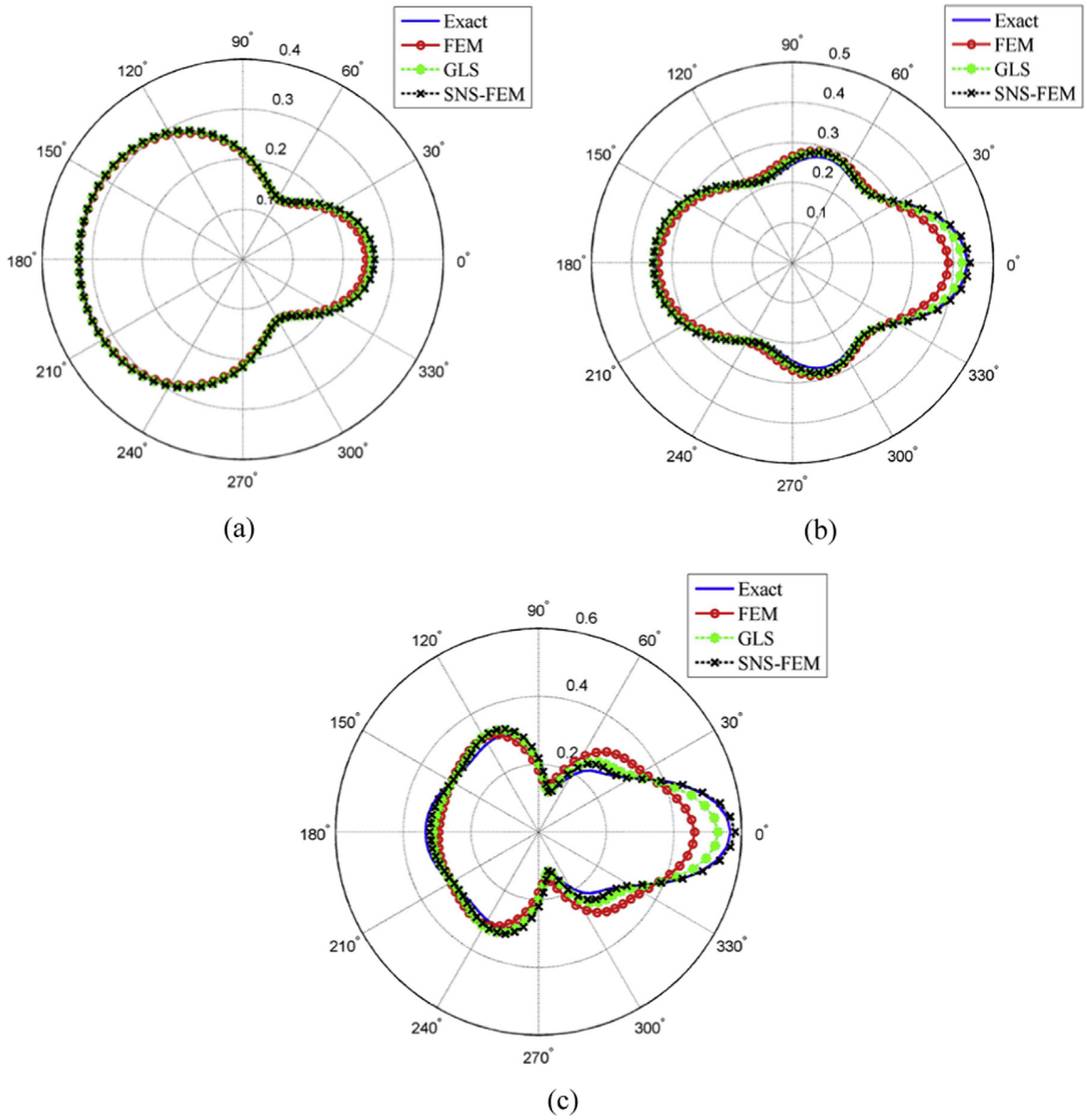

Fig. 6. The scattering patterns of total pressure at a distance of r=1 m at different wave numbers for the circular cylinder: (a) k = 5; (b) k = 10;(c) k = 15.

and accurate numerical results for the acoustic scattering problems.

2. For small wave number, the three models, including the SNS-FEM, FEM and GLS, can provide very accurate results which are in good agreement with the exact solutions and all the numerical errors from different models are small.
3. With the increase of the wave number, all the results from different numerical methods will depart from the exact one and the corresponding numerical errors become larger. However, the SNS-FEM model can obtain much more accurate numerical results than the standard FEM model. More importantly, the SNS-FEM model even can achieve better results than the GLS model which has been proved to be a very effective method to control the numerical error for acoustic problems.

Moreover, the scattered acoustic pressure distribution in the problem domain are also presented. Two different wave number (k = 5 and k = 12) are studied in this model. Fig. 7a and b display the scattered acoustic pressure distribution for k = 5 obtained from SNS-FEM and FEM with the same mesh, while the results using SNS-FEM and FEM for k = 12 are presented in Fig. 8a and b. For the purpose of comparison, the analytical solution of this problem for k = 5 and k = 12 are also plotted in Fig. 7c and Fig. 8c. From the figures, it is observed that SNS-FEM and FEM provide similar results which are in perfect accord with the exact solution for small wave number (k = 5). When it comes to large wave number (k = 12), the contour of the acoustic pressure obtained from SNS-FEM will stand out and are more accurate than the results from FEM compared with the exact solution. From the above results, it is again verified that SNS-FEM performs better than FEM and can achieve more accurate results for acoustic scattering problems, especially for large wave numbers.

Furthermore, the computational efficiency of the present SNS-FEM is also investigated. Here four different meshes are employed to discretize the problem domain. All the program used in this work are compiled by a personal computer with Intel (R) Core (TM) 4 Duo CPU 3.5 GHz and RAM 16 GB. Fig. 9 illustrates the CPU time (s) against the numerical error indicator obtained from different numerical methods at the wave number k = 15. It is observed that the computing load of the SNS-FEM is always larger than those of the GLS and FEM for a

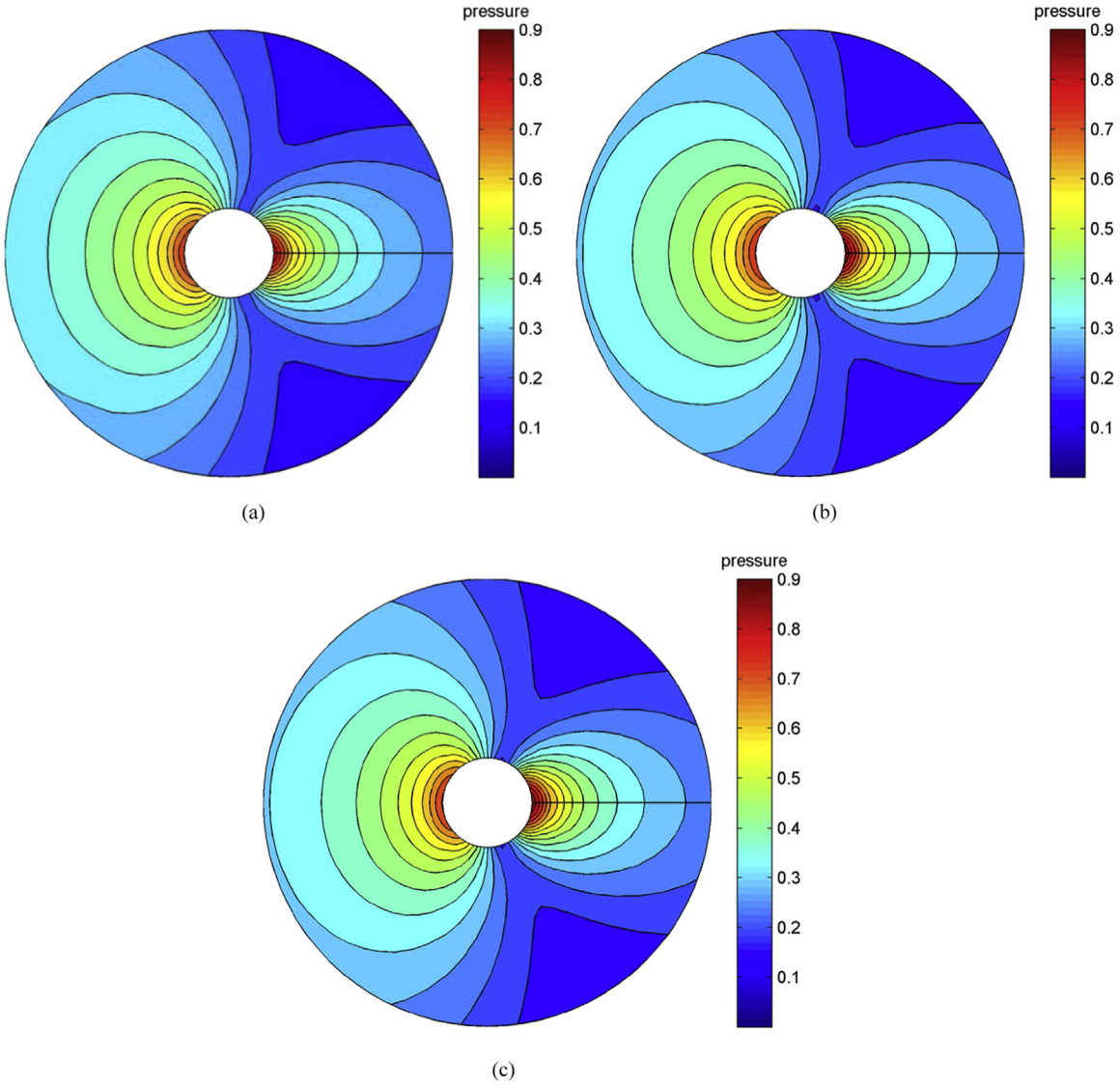

Fig. 7. Scattered acoustic pressure distribution obtained from different numerical methods for wave number $k = 5$: (a) FEM. (b) SNS-FEM. (c) Exact solution.

fixed mesh. This is not difficult to understand. Firstly, performing the node-based smoothing technique over the problem domain needs some additional pre-processing. On the other hand, the bandwidth of the SNS-FEM stiffness matrix is always larger than FEM because in the SNS-FEM model more node information are needed to assemble the element stiffness matrix. These two factors are the main reasons why the SNS-FEM needs more time than FEM with the same mesh. However, it does not mean that the SNS-FEM is not effective enough. When the numerical error indicator is taken into consideration, it is shown from the figure that the SNS-FEM will exhibit higher computational efficiency than GLS and FEM. For example, when the numerical error indicator $E_p = 10^{-6.8}$, the CPU time of SNS-FEM $t_{\mathrm{SNS-FEM}}$ is $10^{-0.3} = 0.50$ s, while the CPU time of the GLS and FEM is $t_{\mathrm{GLS}} = 10^{0.35} = 2.24$ s and $t_{\mathrm{FEM}} = 10^{0.7} = 5.01$ s. It is clear that the CPU time of SNS-FEM is about $1/4$ of the GLS and $1/10$ of the FEM. Therefore, it can be concluded that SNS-FEM is more effective than GLS and FEM.

7.1.2. Convergence study

The convergence of the numerical results from different methods for the acoustic scattering problem will be discussed by using several different meshes. Fig. 10 presents the convergence curves in terms of the relative error against the average mesh size h at different wave number of $k = 10$ and $k = 20$. In order to give a comparison, the SNS-FEM results, together with the FEM and GLS results, are plotted in the figure. From the figure, we may find the following:

1. At small wave number values, the relative errors from all the different methods are small even if the average mesh size is large.
2. With the increase of wave number, the relative errors of all the three methods will increase quickly compared to those of small wave number with the same mesh. However, SNS-FEM is more efficient and can provide better results than FEM and GLS.
3. For a fixed wave number, the relative error of all the numerical methods trend to zero when the mesh gets finer. However, among the three models, the SNS-FEM model stands out very clearly for this problem and converge to the exact solution much faster than FEM and GLS models.

In addition, for the wave number $k = 15$, the convergence rate of the present SNS-FEM is also considered. Fig. 11 gives the convergence rate curves of the three numerical methods. From the figure, it is clear that the SNS-FEM shows a significantly improved performance compared to GLS and FEM.

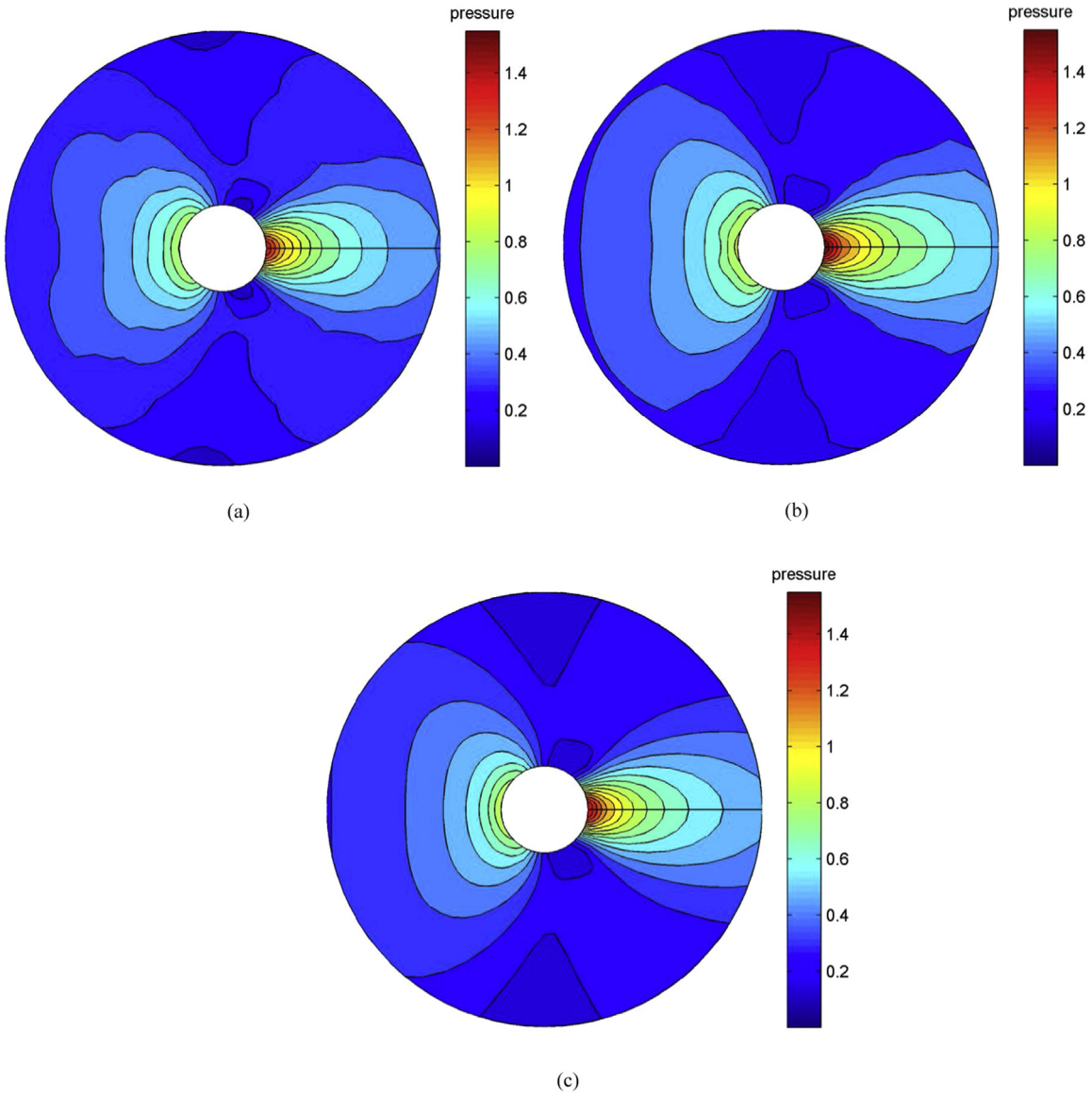

Fig. 8. Scattered acoustic pressure distribution obtained from different numerical methods for wave number $k = 12$: (a) FEM. (b) SNS-FEM. (c) Exact solution.

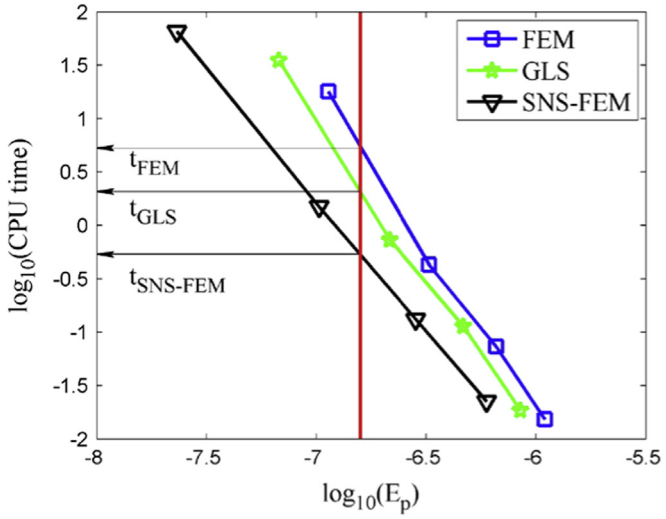

Fig. 9. The CPU time (s) against the numerical error indicator obtained from different numerical methods.

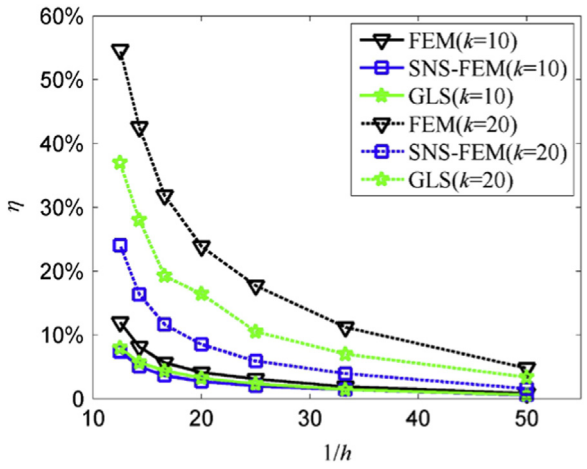

Fig. 10. Comparison of convergence of the results from the three different numerical models with different meshes.

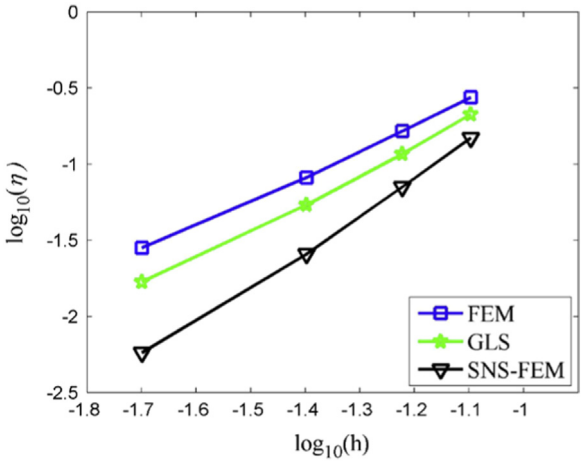

Fig. 11. The convergence rate curves of the three numerical methods.

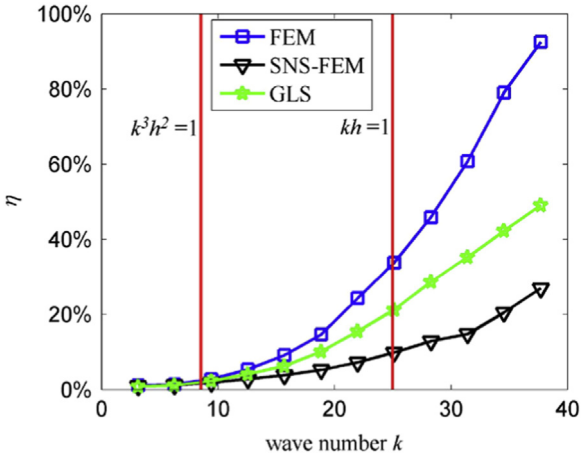

Fig. 12. The global numerical error in the H^1 semi-norm against the wave number k for the different numerical models.

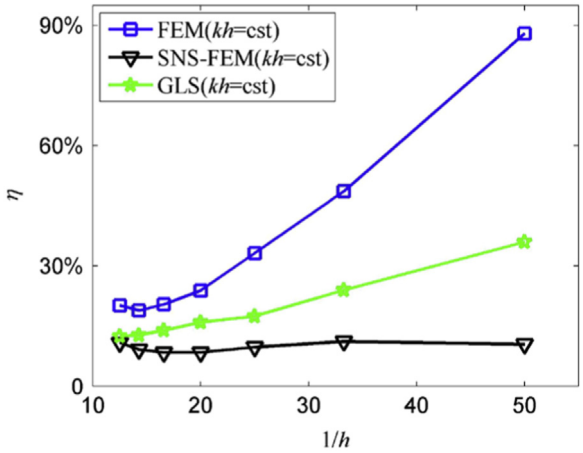

Fig. 13. Evolution of the relative error in H^1 semi-norm against $1/h$ with varying h and keeping kh constant.

7.1.3. Control of the numerical error

From Eq. (35), it is seen that the relative error for acoustic problems is related to the non-dimensional wave number terms kh and k^3h^2. The interpolation error can be controlled by keeping kh constant and the pollution error can be controlled by keeping k^3h^2 constant. In this sub-section, the ability of controlling the relative error for the present SNS-FEM model will be studied. For a fixed

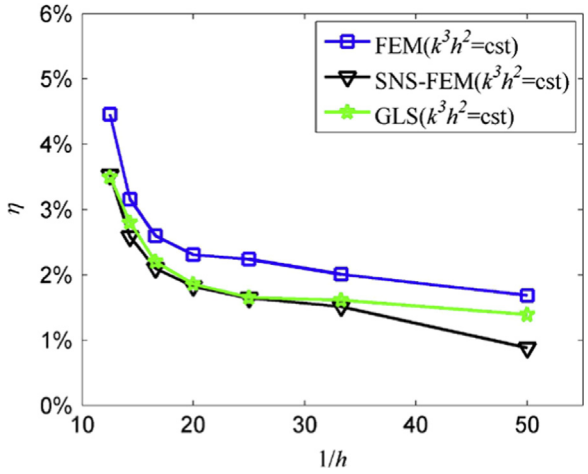

Fig. 14. Evolution of the relative error in H^1 semi-norm against $1/h$ with varying h and keeping k^3h^2 constant.

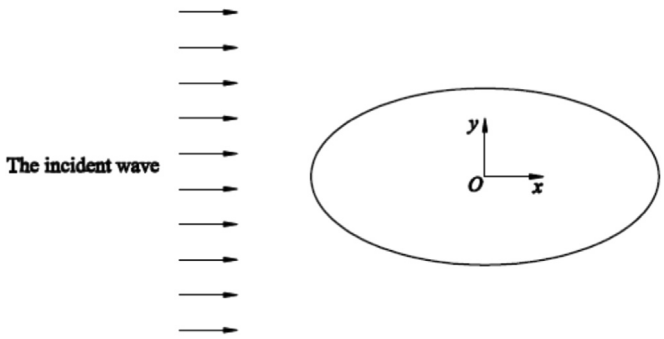

Fig. 15. The geometric shape of the rigid elliptical scatterer.

mesh size, Fig. 12 presents the relative error as a function of the wave number for the three numerical models. For the purpose of discuss, cases of $kh = 1$ (the interpolation error) and $k^3h^2 = 1$ (the pollution error) are also plotted in the figure. As shown in the figure, at very small wave number values, the relative error for all the three models are very small, but the relative error grows quickly as the wave number k increases. However, the GLS results are better than the FEM and worse than the SNS-FEM for the full wave number range. These findings again indicate that SNS-FEM model is reliable and can provide better than FEM and GLS models for acoustic scattering problems.

Furthermore, in order to study the controll of numerical error with the present method clearly. The global numerical errors are calculated using a series of different meshes by keeping kh = cst and k^3h^2 = cst. Fig. 13 shows the relative error as a function of $1/h$ with varying h and keeping kh constant using the above-mentioned three numerical models. From the relative error results in Fig. 13, it is observed that:

1. For small wave number values, the relative error is controlled; the possible reason for this is that the numerical error is mainly from the interpolation error (the first term in Eq. (34)) and the pollution error (the second term in Eq. (34)) can be negligible for small wave number range, while the interpolation error has been controlled by keeping kh constant, hence the relative error is well controlled.
2. For large wave number values, the relative error results will increase dramatically; the reason for this may be that the pollution error will dominate the relative error because the pollution error will increase linearly with the wave number k even

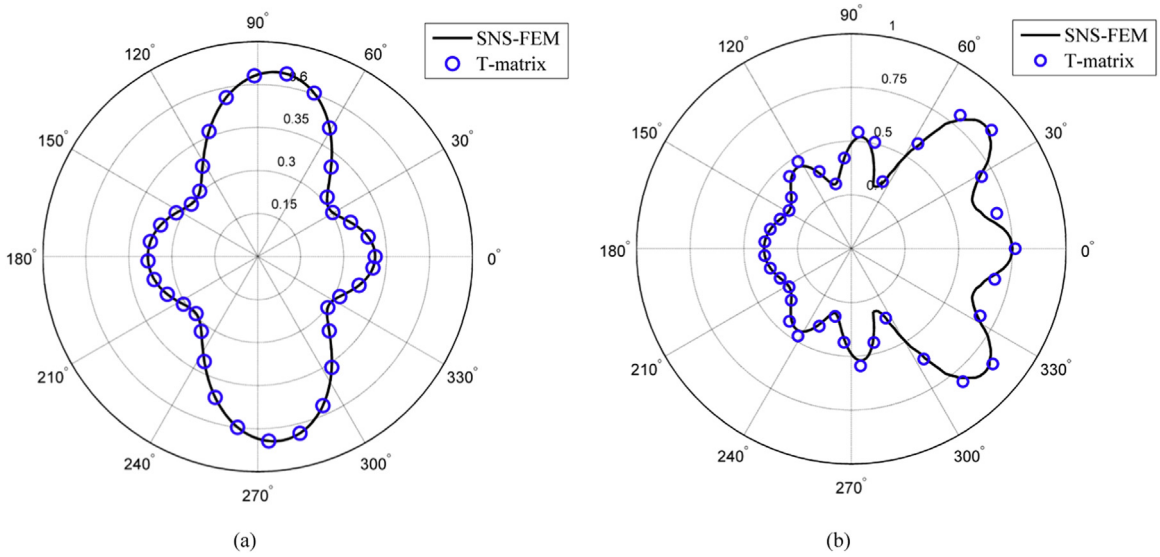

Fig. 16. The scattering pattern at different non-dimensional wave numbers for the elliptical scatterer: (a) $ka = 2$ (b) $ka = 5$.

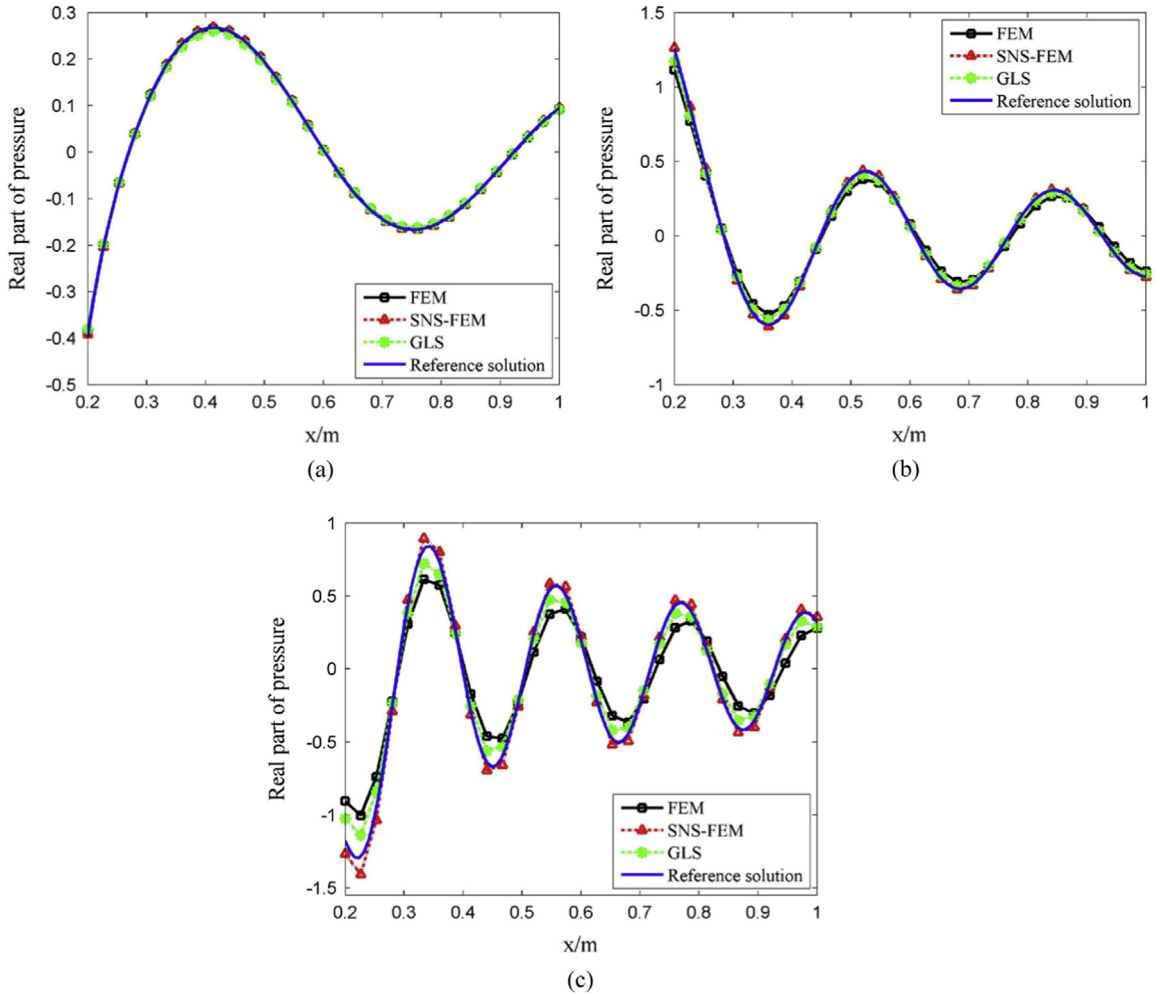

Fig. 17. The real part of the scattered acoustic pressure along the x-axis at different wave numbers for the rigid elliptical scatter: (a) $k = 10$ (b) $k = 20$ (c) $k = 30$.

if kh = cst is kept.

3. Although the relative error from all the three models will increase when the wave number grows, the SNS-FEM model still can give much better results than FEM and GLS models. This means that a certain level of numerical error has been controlled by the node-based gradient smoothing techniques used in the SNS-FEM model.

Fig. 14 shows the relative error as a function of $1/h$ by varying h and keeping k^3h^2 constant. From the figure, it can be seen that the

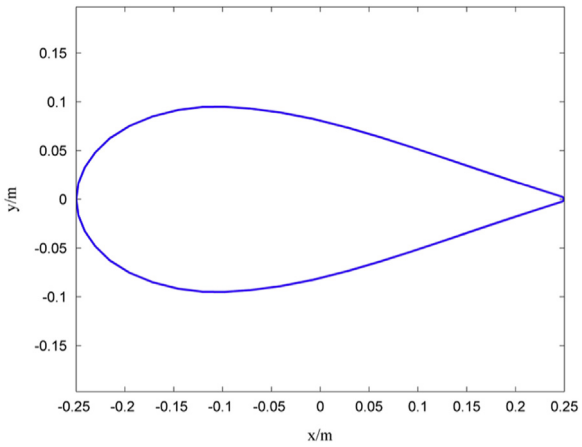

Fig. 18. The geometry of the rigid rudder-shaped scatterer.

relative error can be well controlled for all the three numerical models if k^3h^2 = cst is kept. This is because both the interpolation error and the pollution error can be controlled in the case k^3h^2 = cst based on Eq. (34). However, compared to FEM and GLS models, the SNS-FEM model still provide much better results.

7.2. The elliptical scatterer

In this section, a rigid infinite elliptical cylinder is considered to check and verify the validity of the proposed SNS-FEM model for acoustic scattering problems. The geometric parameters of this problem is shown in Fig. 15, the scatterer located at (0,0) is a rigid elliptical cylinder with an aspect ratio $a/b = 2$ ($a=0.2$ and $b=0.1$). The artificial boundary B is still a circle of radius $R=1$ with center at (0, 0). The incident plane wave and fluid medium are the same as the problem discussed in previous section. The computational domain is discretized into 1480 nodes and 2800 triangular elements.

To illustrate the effectiveness and feasibility of the present method for acoustic scattering problems, the scattering pattern at different non-dimensional wave numbers ($ka=2$ and $ka=5$) for the elliptical scatterer are also calculated. In Fig. 16a and b, the SNS-FEM results were presented in comparison with the numerical results obtained from the well known T-matrix method [52]. It is seen that the SNS-FEM results match fairly well with those obtained from the T-matrix method. Based on the tests and comparisons described above, it is demonstrated that the present SNS-FEM model is effective to solve the acoustic scattering problems.

Furthermore, the numerical results obtained from the three models, including the SNS-FEM, FEM and GLS, will be compared and discussed in this part. Fig. 17 illustrate the real part of the scattered acoustic pressure along the x-axis at different wave

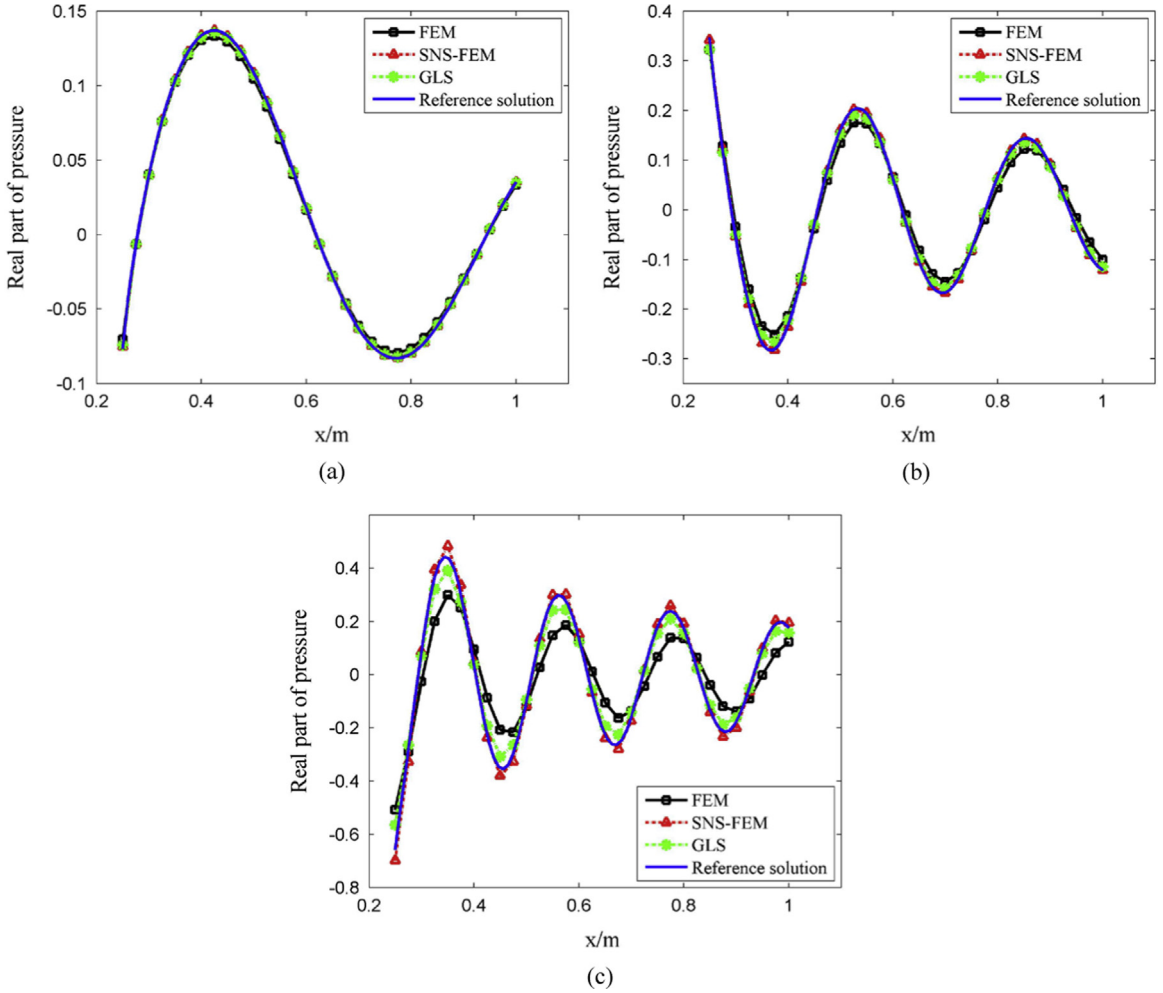

Fig. 19. The real part of the scattered acoustic pressure along the x-axis at different wave numbers for the rudder-shaped scatterer: (a) $k = 10$ (b) $k = 20$ (c) $k = 30$.

numbers ($k = 10$, $k = 20$ and $k = 30$). In order to give a comparison, the numerical results obtained from FEM with a very fine mesh are presented as the reference solutions. As shown in these figures, compared to the SNS-FEM model, the FEM model is able to provide similar numerical results for small wave number range. When it comes to large wave number range, the FEM results will deteriorate quickly. However, the SNS-FEM can provide very accurate results for the full wave number range. More importantly, the numerical results from SNS-FEM model are also much more accurate than those from GLS model. These findings validate that the present SNS-FEM can achieve more stable solutions than FEM and GLS for acoutic scattering problems, especially for large wave numbers.

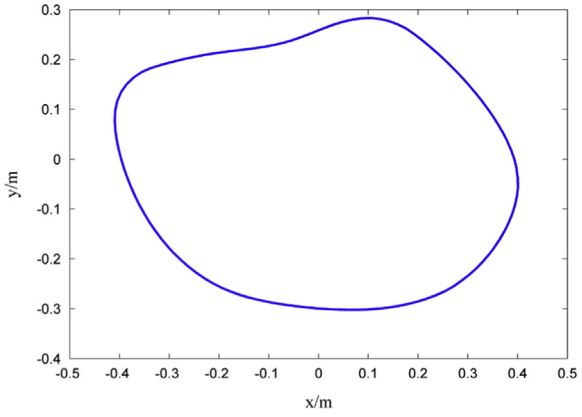

Fig. 20. The geometry of an object of arbitrary shape.

7.3. The rigid rudder-shaped scatterer

To illustrate the performance and ability of the SNS-FEM model for a real structure, the acoutic wave scattering from a rigid rudder-shaped scatterer is investigated in this section. Fig. 18 shows the numerical model. The problem domain is discretized into 1557 nodes and 2970 triangular elements and three different wave numbers ($k = 10$, $k = 20$ and $k = 30$) are considered here. The boundary condition and the incident acoustic wave are the same as described in previous section. The real part of scattered acoustic pressure distribution results along the x-axis obtained from the above-mentioned three models are shown in Fig. 19. Likewise, the reference results obtained from FEM with a very fine mesh are plotted in the figure for comparison. As depicted in the figure, the errors of the real part of the scattered acoustic pressure obtained from the three numerical models are similar to the reference results at small wave numbers. However, for large wave numbers, the numerical results from the SNS-FEM model will depart a little from the reference results, but much less than those from FEM and GLS models. From this numerical example, it is again verified that the SNS-FEM model performs better than FEM and can be used to solve acoustic scattering problems from practical objects with complicated geometry.

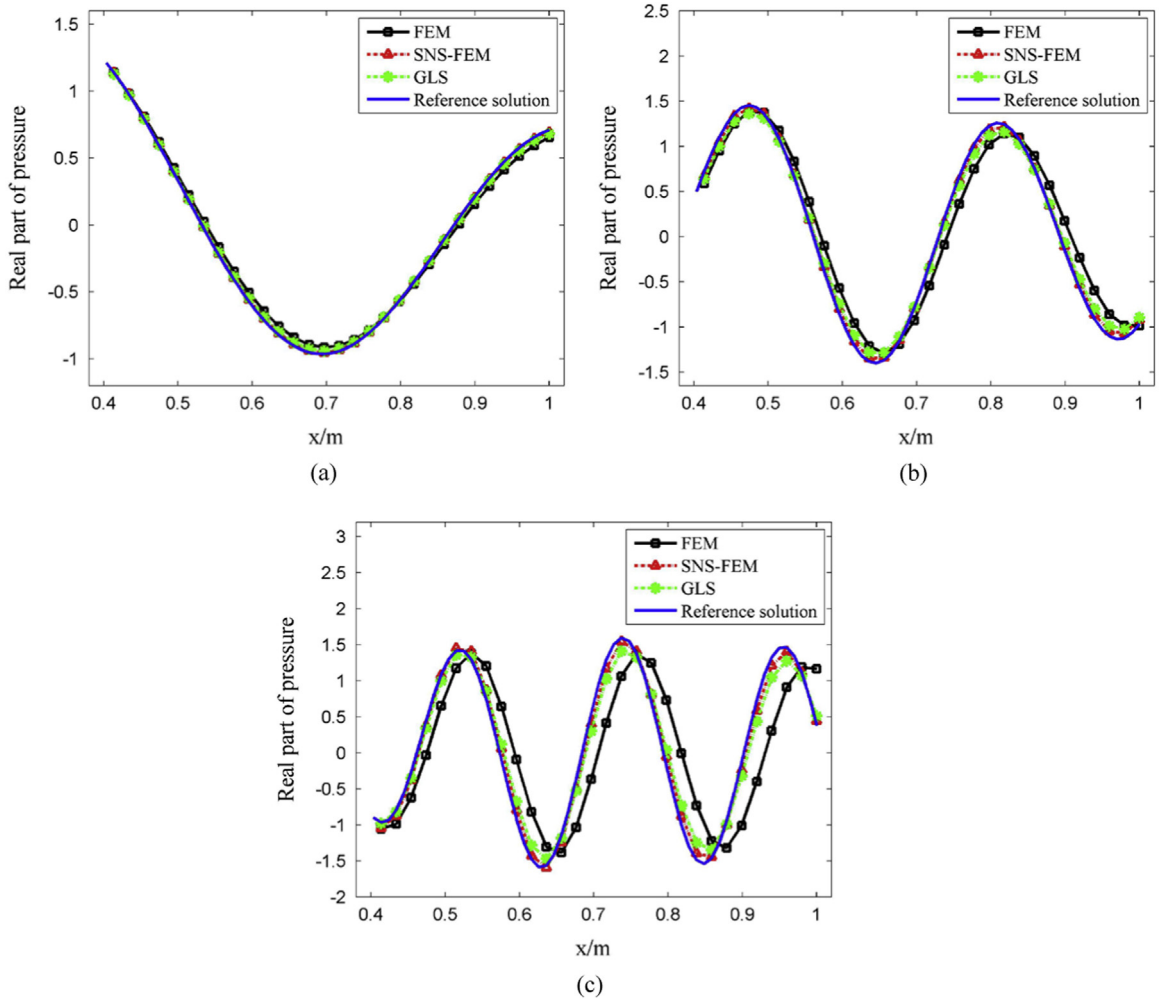

Fig. 21. The real part of the scattered acoustic pressure along the x-axis at different wave numbers for the object of arbitrary shape: (a) $k = 10$ (b) $k = 20$ (c) $k = 30$.

7.4. The object of arbitrary shape

An object of arbitrary shape shown in Fig. 20 is considered here to again test the present SNS-FEM formulation. The surface of the object is rigid. The incident plane acoustic wave is along the x-axis. The radius of the circular artificial boundary B is still $R=1$ and its center is (0, 0). The properties of the fluid around the object are unchanged from the previous numerical examples. The problem domain is discretized into 2266 nodes and 4312 elements. The scattered acoustic distribution results along x-axis are calculated and discussed here. The real part of the acoustic pressure obtained from the three numerical methods at different wave numbers are shown in Fig. 21. Note that the exact solution to this problem is not available, the reference solutions shown in the figures are obtained from FEM using a very fine mesh. From the results shown in Fig. 21, similar conclusions as the previous section can be found. This example again verified that the present SNS-FEM performs better than FEM and GLS and it is very promising to solve more complicated and practical engineering problems.

8. Conclusions

In this paper, the stable node-based smoothed finite element method (SNS-FEM) is formulated and combined with the Dirichlet-to-Neumann (DtN) boundary condition to give a novel SNS-FEM-DtN model for two-dimensional underwater acoustic problems. The numerical integration is implemented over the smoothing domains associated with the nodes of the triangular elements and then the obtained node-based smoothed gradient field is enhanced by the additional stabilization term related to the gradient variance items. A number of numerical examples are investigated in detail to examine the accuracy, convergence and numerical error controll of the present SNS-FEM model. The following conclusions can be drawn from the numerical results.

1. The numerical results from the original NS-FEM for acoustic scattering problems are non-converging due to the “overly-soft” property of the NS-FEM. However, this fatal drawback has been cured by the SNS-FEM model and the SNS-FEM model can provide very stable and convergent results.
2. For acoustic scattering problems, the results of SNS-FEM are in good agreement with the exact solutions and the results of other methods, such as the FMM and T-matrix method. More importantly, the SNS-FEM model shows higher rate of convergence and is much more accurate than the standard FEM the well-known GLS model.
3. The SNS-FEM model works very well with the triangular mesh and no additional parameters or degree of freedoms are needed, hence it can be implemented directly with little change to the original FEM and NS-FEM code.
4. For the practical underwater acoustic scattering problems with complicated geometry, the SNS-FEM performs better than the FEM with the same mesh. It indicates that the SNS-FEM is capable of solving the real engineering problems with very accurate results.

Acknowledgments

The authors wish to express their gratitude to the National Natural Science Foundation of China (Contract No. 51379083, 51579109 and 51579112).

References

[1] Faran Jr JJ. Sound scattering by solid cylinders and spheres. J Acoust Soc Am 1951;23:405–18.
[2] Rudgers AJ. Separation and analysis of the acoustic field scattered by a rigid sphere. J Acoust Soc Am 1972;52:234–46.
[3] Junger MC. Sound scattering by thin elastic shells. J Acoust Soc Am 1952;24:366–73.
[4] Junger MC. The concept of radiation scattering and its application to reinforced cylindrical shells. J Acoust Soc Am 1953;25:899–903.
[5] Silbiger A. Scattering of sound by an elastic prolate spheroid. J Acoust Soc Am 1963;35:564–70.
[6] Burke JE. Long-wavelength scattering by hard spheroids. J Acoust Soc Am 1966;40:325–30.
[7] Yeh C. Perturbation method in the diffraction of electromagnetic waves by arbitrarily shaped penetrable obstacles. J Math Phys 1965;6:2008–13.
[8] Goel GC, Jain DL. Scattering of plane waves by a penetrable elliptic cylinder. J Acoust Soc Am 1981;69:371–9.
[9] Su JH, Varadan VV, Varadan VK, Flax L. Acoustic wave scattering by a finite elastic cylinder in water. J Acoust Soc Am 1980;68:686–91.
[10] DiPerna DT, Stanton TK. Sound scattering by cylinders of noncircular cross section: A conformal mapping approach. J Acoust Soc Am 1994;96:3064–79.
[11] Smith MJA, Meylan MH, McPhedran RC. Scattering by cavities of arbitrary shape in an infinite plate and associated vibration problems. J Sound Vib 2011;330:4029–46.
[12] Mitri FG. Resonance scattering and radiation force calculations for an elastic cylinder using the translational addition theorem for cylindrical wave functions. AIP Adv 2015;5:097205.
[13] Mitri FG. Acoustic backscattering and radiation force on a rigid elliptical cylinder in plane progressive waves. Ultrasonics 2016;66:27–33.
[14] Mitri FG. Acoustic scattering of a cylindrical quasi-Gaussian beam with arbitrary incidence focused on a rigid elliptical cylinder. J Appl Phys 2015;118:184902.
[15] Mitri FG. Acoustic radiation force on a rigid elliptical cylinder in plane (quasi) standing waves. J Appl Phys 2015;118:214903.
[16] Fu ZJ, Chen W, Lin J, Cheng AHD. Singular boundary method for various exterior wave applications. Int J Comput Methods 2015;12:1550011.
[17] Fu ZJ, Chen W, Chen JT, Qu WZ. Singular boundary method: three regularization approaches and exterior wave applications. CMES-Comp Model Eng Sci 2014;99:417–43.
[18] Fu ZJ, Chen W, Gu Y. Burton-Miller-type singular boundary method for acoustic radiation and scattering. J Sound Vib 2014;333:3776–93.
[19] Keller JB, Givoli D. Exact non-reflecting boundary conditions. J Comput Phys 1989;82:172–92.
[20] Bayliss A, Gunzburger M, Turkel E. Boundary conditions for the numerical solution of elliptic equations in exterior regions. SIAM J Appl Math 1982;42:430–51.
[21] Berenger JP. A perfectly matched layer for the absorption of electromagnetic waves. J Comput Phys 1994;114:185–200.
[22] Hastings FD, Schneider JB, Broschat SL. Application of the perfectly matched layer (PML) absorbing boundary condition to elastic wave propagation. J Acoust Soc Am 1996;100:3061–9.
[23] Turkel E, Yefet A. Absorbing PML boundary layers for wave-like equations. Appl Numer Math 1998;27:533–57.
[24] Thompson LL, Pinsky PM. A Galerkin least-squares finite element method for the two-dimensional Helmholtz equation. Int J Numer Methods Eng 1995;38:371–97.
[25] Harari I, Hughes TJR. Galerkin/least-squares finite element methods for the reduced wave equation with non-reflecting boundary conditions in unbounded domains. Comput Meth Appl Mech Eng 1992;98:411–54.
[26] Harari I, Nogueira CL. Reducing dispersion of linear triangular elements for the Helmholtz equation. J Eng Mech 2002;128:351–8.
[27] Babuška I, Ihlenburg F, Paik ET, Sauter SA. A generalized finite element method for solving the Helmholtz equation in two dimensions with minimal pollution. Comput Meth Appl Mech Eng 1995;128:325–59.
[28] Babuška I, Sauter SA. Is the pollution effect of the FEM avoidable for the Helmholtz equation considering high wave numbers? SIAM Rev 2000;42:451–84.
[29] Franca LP, Farhat C, Macedo AP, Lesoinne M. Residual-free bubbles for the Helmholtz equation. Int J Numer Methods Eng 1997;40:4003–9.
[30] Biermann J, von Estorff O, Petersen S, Wenterodt C. Higher order finite and infinite elements for the solution of Helmholtz problems. Comput Meth Appl Mech Eng 2009;198:1171–88.
[31] Belytschko T, Lu YY, Gu L. Element-free Galerkin methods. Int J Numer Methods Eng 1994;37:229–56.
[32] Bouillard P, Suleaub S. Element-Free Galerkin solutions for Helmholtz problems: formulation and numerical assessment of the pollution effect. Comput Meth Appl Mech Eng 1998;162:317–35.
[33] Uras RA, Chang CT, Chen Y, Liu WK. Multiresolution reproducing kernel particle methods in acoustics. J Comput Acoust 1997;5:71–94.
[34] Wenterodt C, von Estorff O. Dispersion analysis of the meshfree radial point interpolation method for the Helmholtz equation. Int J Numer Methods Eng 2009;77:1670–89.
[35] He Z, Li P, Zhao GY, Chen H. A meshless Galerkin least-squares method for Helmholtz equation. Eng Anal Bound Elem 2011;35:868–78.

[36] He ZC, Liu GR, Zhong ZH, Wu SC, Zhang GY, Cheng AG. An edge-based smoothed finite element method (ES-FEM) for analyzing three-dimensional acoustic problems. Comput Meth Appl Mech Eng 2009;199:20–33.
[37] Liu GR, Nguyen-Thoi T, Dai KY, Lam KY. Theoretical aspects of the smoothed finite element method (SFEM). Int J Numer Methods Eng 2007;71:902–30.
[38] Liu GR, Dai KY, Nguyen-Thoi T. A smoothed finite element method for mechanics problems. Comput Mech 2007;39:859–77.
[39] Li Y, Li M, Liu GR. A modified triangulation algorithm tailored for the smoothed finite element method (*s*-FEM). Int J Comput Methods 2014;11:1350069.
[40] Liu GR, Nguyen-Thoi T, Lam KY. An edge-based smoothed finite element method (ES-FEM) for static, free and forced vibration analyses of solids. J Sound Vib 2009;320:1100–30.
[41] Li E, He ZC, Xu X, Liu GR. Hybrid smoothed finite element method for acoustic problems. Comput Meth Appl Mech Eng 2015;283:664–88.
[42] Chai YB, Li W, Gong ZX, Li TY. Hybrid smoothed finite element method for two-dimensional underwater acoustic scattering problems. Ocean Eng 2016;116:129–41.
[43] He ZC, Liu GR, Zhong ZH, Zhang GY, Cheng AG. A coupled ES-FEM/BEM method for fluid–structure interaction problems. Eng Anal Bound Elem 2011;35:140–7.
[44] Li W, Chai YB, Lei M, Liu GR. Analysis of coupled structural-acoustic problems based on the smoothed finite element method (*s*-FEM). Eng Anal Bound Elem 2014;42:84–91.
[45] Wang G, Cui XY, Liang ZM, Li GY. A coupled smoothed finite element method (*s*-FEM) for structural-acoustic analysis of shells. Eng Anal Bound Elem 2015;61:207–17.
[46] Liu GR, Nguyen-Thoi T, Nguyen-Xuan H, Lam KY. A node-based smoothed finite element method (NS-FEM) for upper bound solutions to solid mechanics problems. Comput Struct 2009;87:14–26.
[47] Nguyen-Thoi T, Vu-Do HC, Rabczuk T, Nguyen-Xuan H. A node-based smoothed finite element method (NS-FEM) for upper bound solution to visco-elastoplastic analyses of solids using triangular and tetrahedral meshes. Comput Meth Appl Mech Eng 2010;199:3005–27.
[48] Liu GR, Chen L, Nguyen-Thoi T, Zeng KY, Zhang GY. A novel singular node-based smoothed finite element method (NS-FEM) for upper bound solutions of fracture problems. Int J Numer Methods Eng 2010;83:1466–97.
[49] Wang G, Cui XY, Feng H, Li GY. A stable node-based smoothed finite element method for acoustic problems. Comput Meth Appl Mech Eng 2015;297:348–70.
[50] Feng H, Cui XY, Li GY. A stable nodal integration method with strain gradient for static and dynamic analysis of solid mechanics. Eng Anal Bound Elem 2016;62:78–92.
[51] Ihlenburg F, Babuska I, Sauter S. Reliability of finite element methods for the numerical computation of waves. Adv Eng Softw 1997;28:417–24.
[52] Pillai TAK, Varadan VV, Varadan VK. Sound scattering by rigid and elastic infinite elliptical cylinders in water. J Acoust Soc Am 1982;72:1032–7.